OPEN ACCESS

Biomaterials ARTICLE

The Innovation Materials

Engineering traps in Tm-doped calcium titanate for visible and near-infrared double band persistent luminescence bioimaging

Leping Ding,[1] Juanjuan Zhou,[2,3,*] Gulizhabaier Abulipizi,[1] Ziang Zong,[1] Zihao Chen,[1] Yawen Zheng,[4] Xingyuan Shi,[1] and Zhanjun Li[1,3,*]

*Correspondence: zhanjunli@gzhmu.edu.cn (Z.L.); jjzhou417@163.com (J.Z.)

Received: September 17, 2025; Accepted: January 26, 2026; Published Online: January 26, 2026; https://doi.org/10.59717/j.xinn-mater.2026.100200

GRAPHICAL ABSTRACT

PUBLIC SUMMARY

- Y surpassed Sc, La, Gd, and Lu in enhancing the persistent luminescence (PersL) of $CaTiO_3$:Tm.
- Al, Ga, and In decreased the near-infrared (NIR) PersL of $CaTiO_3$:Tm.
- Three basic laws were derived for optimizing the NIR PersL.
- $CaTiO_3$:Tm, Y, Pr showed visible and NIR PersL at 613 and 803 nm, respectively.
- $CaTiO_3$:Tm, Pr, Y was applied to multi-modal imaging both *in vitro* and *in vivo*.

ARTICLE Biomaterials

OPEN ACCESS

Engineering traps in Tm-doped calcium titanate for visible and near-infrared double band persistent luminescence bioimaging

Leping Ding,[1] Juanjuan Zhou,[2,3,*] Gulizhabaier Abulipizi,[1] Ziang Zong,[1] Zihao Chen,[1] Yawen Zheng,[4] Xingyuan Shi,[1] and Zhanjun Li[1,3,*]

[1]Key Laboratory of Biological Targeting Diagnosis, Therapy and Rehabilitation of Guangdong Higher Education Institutes, The Fifth Affiliated Hospital, School of Biomedical Engineering, Guangzhou Medical University, Guangzhou 511436, China

[2]College of Chemistry and Molecular Sciences, Wuhan University, Wuhan 430072, China

[3]School of Health, Guangzhou Vocational University of Science and Technology, Guangzhou 510080, China

[4]Affiliated Cancer Hospital of Guangzhou Medical University, Guangzhou 510095, China

*Correspondence: zhanjunli@gzhmu.edu.cn (Z.L.); jjzhou417@163.com (J.Z.)

Received: September 17, 2025; Accepted: January 26, 2026; Published Online: January 26, 2026; https://doi.org/10.59717/j.xinn-mater.2026.100200

Citation: Ding L., Zhou J., Abulipizi G., et al. (2026). Engineering traps in Tm-doped calcium titanate for visible and near-infrared double band persistent luminescence bioimaging. *The Innovation Materials* **4**:100200.

$CaTiO_3$:Tm (CTT) has unusual red-light charged near-infrared (NIR) persistent luminescence (PersL) property at ~ 800 nm. In this study, trap engineering was realized by co-doping CTT with 8 non-luminescent trivalent ions. Some basic laws in optimizing the NIR PersL of CTT were established based on the observation that rare earth dopants, including Sc/Y/La/Gd/Lu, at the A site of the ABO_3 perovskite structure of $CaTiO_3$ increased the PersL while the boron group dopants, including Al/Ga/In, at the B site led to decreased PersL. Y was found as an efficient co-dopant to realize enhanced NIR PersL in $CaTiO_3$:Tm,Y (CTT-Y) with a ~60% enhancement *vs.* CTT. Thermal-stimulated luminescence (TSL) study indicate that Y is the most efficient element in generating abundant energy traps while slightly increased the trap depth from 320 to 326 K. Further, by choosing Pr as the 3rd dopant, visible-NIR double band fluorescence and PersL was realized in $CaTiO_3$:Tm,Y,Pr (CTT-Y-Pr) at 613 and ~800 nm, which were ~5 and 2 times of those of $CaTiO_3$:Tm,Pr (CTT-Pr), respectively. CTT-Y-Pr was applied to realize four-modal optical anti-counterfeiting imaging *in vitro* including visible fluorescence, visible PersL, invisible NIR fluorescence, and invisible NIR PersL. Moreover, visible fluorescence and NIR PersL imaging *in vivo* was applied to observe implanted tissue filler and its post-surgical tissue cleaning by using CTT-Y-Pr as an optical imaging contrast reagent, which was hard to retrieve once it was injected within body and formed unwanted tiny debris.

INTRODUCTION

Persistent luminescence (PersL or afterglow) is an unusual optical phenomenon in which materials keep glowing photons for seconds or even days after the excitation light or irradiation source is turned off.[1,2] The PersL process looks like a short term charging process for a long term sustained release of stored energy in a rechargeable battery but in a form of emitting photons instead of releasing electrons.[3] The temporally separable excitation/emission attribute of PersL generates a new optical imaging manner termed PersL imaging, which avoids autofluorescence background and expensive time-resolved equipments.[4,5] Near-infrared (NIR) PersL has promising applications in optical bioimaging, tumor therapy, luminescent analysis, radiation detection, anti-counterfeiting painting, and information encryption etc.[6-10] Cr-doped PersL materials have been successfully developed with typical emission peaks at ~700 nm, such as $ZnGa_2O_4$:Cr, $Zn_3Ga_2Ge_2O_{10}$:Cr, and derivatives.[11-14] Nevertheless, new PersL materials are being explored with non-Cr activator ions or non-gallium oxide-derived phosphor matrix, such as $Ca_3Ga_2Ge_3O_{12}$:Bi,[15] CaZnOS:Nd,[16] Sr_2LuSbO_6:Fe[17], Mg_2SnO_4:Cr,[18] La_2CaHfO_6:Cr,[19] $Na_2CaGe_5SiO_{14}$:Cr.[20] Although a bunch of PersL phosphors have been reported, most of them still rely on ultraviolet (UV) light illumination, high power NIR laser, or X-ray irradiation to activate the PersL. Visible-light-chargeable NIR PersL phosphors are still needed to explore their advanced applications in diverse fields.

Titanate-based phosphors, with a perovskite structure, have much lower band gaps than gallium oxide-based phosphors. Doped titanate phosphors were reported with interesting visible-light-chargeable NIR PersL properties. For example, $Na_{0.5}Gd_{0.5}TiO_3$:Cr was firstly reported with red-light-chargeable NIR PersL with an emission peak at 770 nm.[21] A further optimized composition was reported as $Na_{0.5}Y_{0.5}TiO_3$:Cr and applied as a functional coating layer to label a medical titanium plate, which was implanted in a mouse model and showed in situ rechargeable PersL bioimaging property.[22] As the oldest perovskite oxide mineral, $CaTiO_3$ was widely studied as an optical matrix and at the same time showed good biocompatibility. A series of $CaTiO_3$-based NIR PersL materials were reported. $CaTiO_3$:Y was reported with blue-light-chargeable NIR PersL at 770 nm, which was assigned to Ti^{3+} absorption and emission.[23] $CaTiO_3$:Cr,Y was developed with red-light-chargeable NIR PersL at 772 nm and was applied to label a medical bone screw.[24] After being implanted in a porcine limb model, the PersL of the bone screw was *in situ* charged by using a red LED and imaged through 17 mm pork tissue. Recently, $CaTiO_3$:Tm was reported with unusual single band *ca.* 800 nm PersL with a wide charging spectrum from UV to NIR.[25] The narrow PersL band reveals great potential of lanthanide-doped NIR PersL materials in multiple fields from bioimaging to optical devices. In addition, co-doping with other lanthanide ions may generate more energy traps and thus significantly improve its PersL property. Yet, this issue is still not clear. Moreover, $CaTiO_3$:Tm has only one NIR PersL peak which can only be observed by using a NIR camera while keeps invisible to naked eyes. Its applications in advanced multi-level optical encryption, anti-counterfeiting, and multi-modal biomedical imaging are still limited.

Herein, to reveal the trap-adjusting mechanism of trivalent co-dopants in $CaTiO_3$:Tm (CTT), Y/Sc/La/Gd/Lu/Al/Ga/In was used as a non-luminescent trivalent co-dopant to generate a series of $CaTiO_3$:Tm,Ln (CTT-Ln) phosphors. After comparing their PersL properties, an optimized composition, $CaTiO_3$:Tm,Y (CTT-Y), was provided. Further, to realize NIR and visible PersL simultaneously in calcium titanate, Pr was used as the third dopant to produce $CaTiO_3$:Tm,Y,Pr (CTT-Y-Pr) because of its well-known visible PersL at 613 nm. The interactions of Tm, Y, and Pr on their PersL were studied in detail. In this way, multi-modal optical imaging was realized both in the visible by naked eyes and in the NIR by a CCD camera.

MATERIALS AND METHODS

Materials

$CaCO_3$, TiO_2 nanoparticles (100 nm), and H_3BO_3 were A. R. grade and purchased from Sinopharm, China. Thulium acetate (99.9%), yttrium acetate (99.9%), and praseodymium acetate (99.9%) were purchased from Aladdin Reagent, China. The silicone A-B gel (hardness, 15) was purchased from Kerong Biotech, China.

Synthesis of doped $CaTiO_3$

Doped $CaTiO_3$ was synthesized according to a traditional solid state annealing method. Taking $CaTiO_3$:$Tm_{0.01}$,$Y_{0.01}$ (CTT-Y) as an example, TiO_2 (10 mmol), $CaCO_3$ (9.60 mmol), thulium acetate (0.100 mmol), yttrium acetate (0.100 mmol), and H_3BO_3 (0.500 mmol) were mixed by milling using a agate mortar. A Ca deficiency of ~1% was applied to improve the PersL. 5 mL of ethanol was added to assist the milling process. After the ethanol was evaporated and a powder-form mixture was formed, the precursor was trans-

ferred to a corundum crucible, and then annealed at 1373 K for 10 h. The annealed product was milled using a mortar and pestle to obtain the final PersL CTT-Y material.

A series of $CaTiO_3$:Tm, Ln (CTT-Ln) phosphors were synthesized by using the same procedures except that another trivalent ion, Sc/La/Gd/Lu/Al/Ga/In, was used to substitute Y with the same doping concentration (1.00% vs Ti by molar).

To induce visible PersL in $CaTiO_3$, $CaTiO_3$:Pr, and CTT-Y-Pr were synthesized by using the same procedures with a Ca/Ti/Pr/Tm/Y molar ratio of 0.990/1.00/0.0010/0/0 and 0.960/1/0.0010/0.010/0.010, respectively.

Refined powder of CTT-Y-Pr was prepared by using a ball grinding mill for 24 h. The volume of the milling pot was 100 mL. 1 g of phosphor samples were mixed with milling balls of 10 mm (*1), 5 mm (*2), and 2 mm (*200) in diameter, respectively. 3 mL of ethanol was added to assist the milling process.

Preparation of an optical encryption pattern based on CTT-Y, $CaTiO_3$:Pr, and CTT-Y-Pr

A round transparent resin plate with a dented pattern was prepared using a third party 3-D printed service. Refined powder of CTT-Y (~ 100 mg) and CTT-Y-Pr (~ 250 mg) was filled into the diverse parts of the dented pattern to form a luminescent encryption logo.

Preparation of CTT-Y-Pr labeled injectable silicone

Regarding the medical silicone tissue filler imaging demo, CTT-Y-Pr was mixed with medical silicone gel (A-B type, 1:1 by volume) by manually milling for 1 min using a mortar and pestle. The mass content of CTT-Y-Pr was 1 wt%. A 1 mL syringe was used to inject the CTT-Y-Pr/silicone mixture subcutaneously as soon as it was prepared (A gel was formed within ~10 min at room temperature). After 24 h, the mouse was anaesthetized to conduct optical imaging. All animal procedures were applied per a protocol approved by the Institutional Animal Care and Use Committee of Guangzhou Medical University (GY2024-633).

Characterization

Optical spectra, including fluorescence and PersL, of all the doped calcium titanate phosphors were acquired using a fluorospectrophotometer (FS5, Edinburgh Instruments, UK) coupled with a red-sensitive detector (MDL-III-980, Changchun New Industries Optoelectronics Tech., China). Thermo-stimulated luminescence (TSL) was tested with a heating rate of 2 K/s using a thermoluminescence dosimeter equipped with a red sensitive R925 detector (Guangzhou Radiation Co., Ltd. CN). The X-ray patterns (XRD) were acquired using a powder diffractometer (D2-Phaser, Bruker Instruments, Germany). PersL imaging of the CTT-Ln and the multi-modal imaging of the prepared logo were performed using a multifunctional optical imaging system coupled with an OptiChemi 615 CCD camera and blue/red LED arrays with an illumination intensity of ~ 1000 lx (± 100) (UVP Chemstudio Touch, Analytik Jena, Germany). Animal fluorescence/PersL imaging was conducted in an IVIS small animal imaging system (Lumina XRMS Series III, PerkinElmer, USA). The visible fluorescence image and movie were acquired by using a common cell phone camera.

RESULTS

Physical structure of CTT-Ln

XRD was used to confirm the crystal structures of the as synthesized persistent phosphors. As shown in Figure 1A, all the XRD patterns can be assigned to perovskite $CaTiO_3$ without any significant impurity peaks (JCPDS card no. 01-089-8033). The doping with Tm and other trivalent ions haven't led to observable changes in their XRD peaks. Ca^{2+} (0.099 nm) has a similar ionic radii with lanthanide ions (from 0.081 of Sc^{3+} to 0.106 nm of La^{3+}). Thus, lanthanide ions are ease to take the crystal lattice of Ca^{2+} (site A) in $CaTiO_3$ (Figure 1B). On the other hand, Ti^{4+} (0.068 nm) has a similar radii with Al^{3+} (0.050 nm) and Ga^{3+} (0.062 nm), which are supposed to take the lattice of Ti^{4+}. In^{3+}, together with Al^{3+} and Ga^{3+}, belongs to the boron group in the periodic table of elements. Although its ionic radius, 0.081 nm, is closer to that of Ca^{2+} and rare earths, In^{3+} has similar chemical property with Ga^{3+} and is

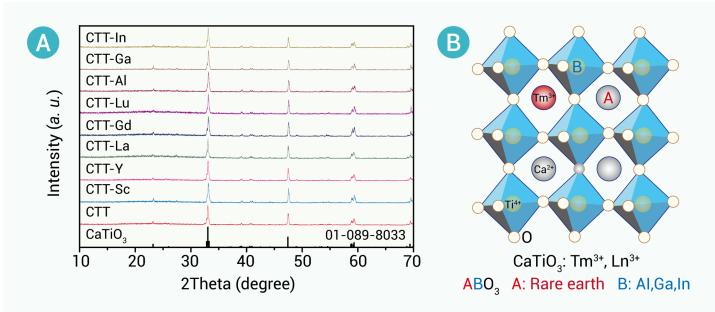

Figure 1. Crystal structure of the as-synthesized CTT-Ln phosphors (A) XRD patterns; (B) schematic illustration of doped perovskite structure.

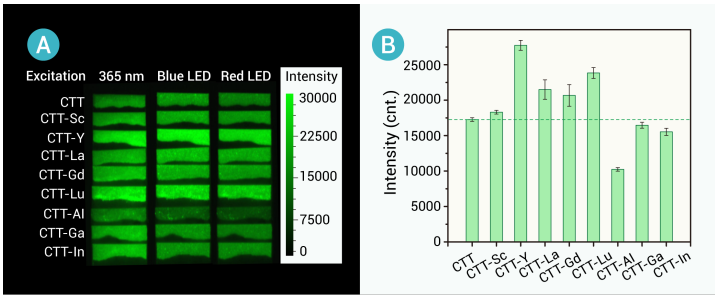

Figure 2. Comparison of the PersL intensities of CTT-Ln with CTT (A) PersL image with intensity shown as false color. The camera exposure time was set to 1 s, 1 s, and 5 s when using 365 nm UV lamp (6 W), blue LED (1000 lx), and red LED (1000 lx) as the excitation light source, respectively; (B) quantitative PersL intensity analysis charged by red LED.

supposed to take the lattice of Ti^{4+} in $CaTiO_3$. As the doping concentration is low, there are no significant difference in their XRD patterns. Or, in other words, the doping of $CaTiO_3$ by trivalent ions are ease to realize by using a simple solid state annealing method.

Superior PersL intensity of CTT-Y *vs.* CTT-Ln

The chosen co-dopants in CTT-Ln have no luminescence in the visible-NIR region. All the CTT-Ln samples exhibit similar single band PersL spectra with a typical emission of Tm^{3+} at ~ 800 nm (Figure S1). No other emission peaks, like the typical blue emission of Tm^{3+} at ~ 458 nm, could be observed, possibly because of the same reason in CTT that trace amount of Ti^{3+} absorbed the blue emission of Tm^{3+} and enhanced its NIR emission.[25]

As there is only a single emission band in all the CTT-Ln phosphors, their initial PersL intensities were compared by using an optical imaging system coupled with a CCD camera (Figure 2A). The results indicate that the as-synthesized CTT-Ln phosphors could be charged not only by UV light (6 W mercury lamp) but also by blue or red light (1000 lx LED array installed in the imaging system). Although less efficient, red light could indeed charge the NIR PersL with an intensity of *ca.* 20% of that charged by using blue light. Notably, all the chosen rare earth ions, Sc/Y/La/Gd/Lu, increased the PersL intensity while Y^{3+} turns out to be the most effective co-dopant in improving the PersL intensity of Tm^{3+} in $CaTiO_3$. In contrast, all the boron group ions, Al/Ga/In, decreased the PersL of CTT (Figure 2B). A possible reason might be that lanthanide ions are supposed to take the A site of the ABO_3 perovskite structure of $CaTiO_3$, while the boron group ions are supposed to take the B site.

The photoluminescence excitation/emission spectra were shown in Figure 3A. All the CTT-Ln samples exhibit similar ex/em spectra, except for a little difference in the excitation spectra below 450 nm. The small excitation peaks at ~420 nm are attributed to the $^2T_2 - {}^2E$ transition of Ti^{3+}. CTT-Y happens to possess the most intense excitation intensity at this wavelength while CTT-Al has the weakest, which coincides with the optimized and the weakest PersL of CTT-Y and CTT-Al, respectively (Figure 3B). Moreover, Y-doping slightly decreased the band gap of CTT from from 3.41 eV to 3.32 eV (Figure S2), which may result in improved interaction of the conduction band of $CaTiO_3$

and the energy levels of lanthanide ions and Ti^{3+}. Therefore, Y turns out to be an efficient co-dopant in generating Ti^{3+} in $CaTiO_3$, while in contrast, Al hinders the Ti^{3+} generation.

Energy traps in CTT-Ln charged by red-light illumination

Thermal-stimulated luminescence (TSL) intensity was tested with a heating rate of 2 K/s. The results indicate that co-doping CTT with none luminescent trivalent ions significantly influenced the TSL peak intensity while only slightly influenced the peak position (Figure 4A). The most intense TSL of CTT-Y indicates that Y is the most efficient dopant in generating energy traps among the chosen Ln^{3+}. Notably, the doping of Al strongly inhibited the generation of energy traps, which is different from existing reports that Al enhanced the UV-charged red PersL of Pr in $CaTiO_3$:Pr, Al.[26,27] Thus, the influence of lanthanide ions on the NIR PersL of CTT might follow different laws that were found in $CaTiO_3$:Pr and needs further study. In addition, the TSL peak of CTT-Y slightly shifted to a higher temperature from 320 K to 326 K, the highest TSL in all the CTT-Ln samples, which means deeper trap energy level and makes it more suitable for long term PersL applications (Figure 4B). According to our previous report, the PersL of CTT originates from the trapping of electrons, which are generated by excited Ti^{3+}, in oxygen vacancy. As CTT-Y has the most intense TSL peak and PersL intensity at room temperature, Y turns out to be the most efficient co-dopant in generating oxygen vacancy, stabilizing trace Ti^{3+}, and adjusting the trap to a deeper energy level.

The PersL decay curve of CTT-Y was compared with CTT (Figure S3). The kinetic decay lifetime factors were fitted by using a double-exponential decay model from their PersL decay curves (Table S1). After being charged by a red LED, CTT-Y not only possesses higher initial PersL intensity ($A_1 + A_2$), corresponding to its higher TSL peak value, with an enhancement of *ca.* 45%, but also longer lifetime factors of t_1 from 34 to 38 s and t_2 from 282 to 343 s. Notably, as the PersL of CTT-Y is easily re-chargeable by biocompatible red light, a short PersL lasting time of several minutes are already able to meet the requirements of most imaging-related applications, especially at biological environment.

Proposed mechanism on the superior PersL of CTT-Y

Rare earth and alkali earth ions have similar ionic radii. Thus, Ca-based materials are frequently studied as rare earth-doped phosphor matrix, such as CaF_2:Dy@$NaYF_4$,[28] CaO:Eu,[29] CaS:Eu,[30] $CaAl_2Si_2O_8$:Eu,[31] and $Ca_3(PO_3)_2$.[32,33] A general law is found that co-doping with Sc/Y/La/Gd/Lu enhances the PersL of CTT while co-doping with Al/Ga/In decreases the PersL of CTT (Figure 5A). After comparing the selected rare earth with Ca, Y^{3+} happens to possess the most similar ionic radii with Ca^{2+}. This might result in the highest doping efficiency in CTT-Y and thus the most intense PersL intensity. Al/Ga/In belongs to the boron group elements and are supposed to take place the Ti lattice in CTT-Ln. Existing studies found that co-doping with Al^{3+} lead to enhanced UV-charged PersL intensity in $CaTiO_3$:Pr.[26] However, in the case of CTT, Al/Ga/In decreased the red-light charged PersL of CTT as a co-dopant, which was quite different from Y. A possible reason might be that Al/Ga/In, as a trivalent ion, is supposed to take place of Ti^{4+} lattice. Al/Ga/In at the B site in the ABO_3 perovskite structure of $CaTiO_3$ acts as a fake Ti^{3+} and will decrease the amount of Ti^{3+} caused by Tm^{3+}-doping at the A site of $CaTiO_3$. According to our previous study, Ti^{3+}, induced by Tm-doping, plays a key role in the PersL of CTT.[25] Therefore, Doping with Al/Ga/In will decrease the PersL of CTT by decreasing the amount of Ti^{3+}. These data further confirm the unusual role of Y^{3+} in PersL CTT-Y.

Some basic laws are induced to improve the PersL of CTT with an ABO_3 perovskite structure by co-doping (Figure 5B), including: (i) Doping at the A site enhances the PersL by generating more Ti^{3+} due to charge compensation,[23,34] (ii) Doping at the B site decreased the PersL by competing with Ti^{3+}. (iii) The doping process has a similar ionic size priority that the codopant radii should be close to that of A^{2+}. For example, Sc^{3+} has the smallest radius and exhibited poor PersL enhancement comparing with CTT-Y, CTT-Gd, and CTT-Lu. (iv) The doping process prefers dopants with similar atomic numbers. For example, Y^{3+}, Gd^{3+}, and Lu^{3+} have quite similar ionic radii and CTT-Y possesses the most intense PersL. An ideal co-dopant will be a trivalent ion with the same radius of Ca^{2+} and the same atomic number. Due to the limited elemental choice, Y^{3+} turns out to be the closest one to the ideal choice. Notably, these basic laws are based on our observation on the co-doing effect of trivalent ions in CTT-Ln phosphors. This finding is significant to facilitate the material designing process of other latent NIR PersL perovskites.

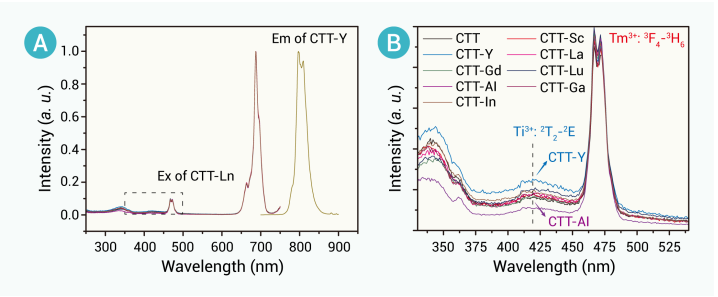

Figure 3. Photoluminescence spectra of CTT-Ln (A) Excitation spectra of CTT-Ln (em, 800 nm) normalized to the 688 nm peak and the emission spectrum of CTT-Y (ex, 688 nm); (B) zoom-in of the selected excitation spectra in (B).

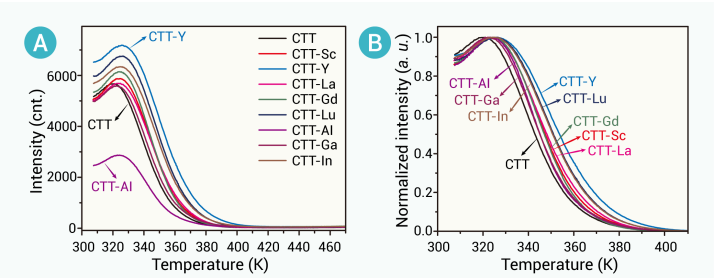

Figure 4. Thermal-stimulated luminescence of CTT-Ln phosphors charged by a 365 nm UV lamp (A) Original TSL curves; (B) normalized TSL curves.

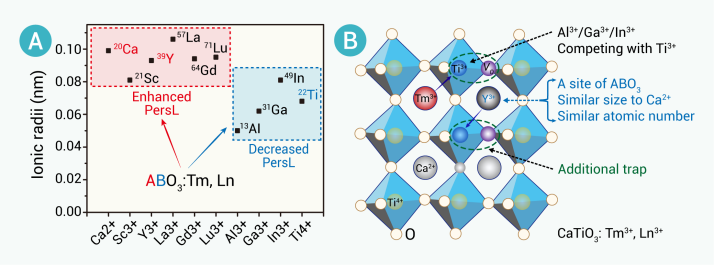

Figure 5. Proposed mechanism of the influence of Ln^{3+} co-doping in PersL CTT-Ln (A) Ionic radii comparison of the selected trivalent ions with Ca^{2+} and Ti^{4+}; (B) laws in optimizing the PersL of CTT-Ln.

Visible-NIR double band PersL of CTT-Y-Pr

$CaTiO_3$:Pr has a known UV-charged PersL peak at ~613 nm.[35] After doping CTT-Y with Pr, visible-NIR double band PersL was realized in CTT-Y-Pr at 613 nm and 803 nm (Figure 6A). The PersL spectra of CTT-Y-Pr were significantly influenced by charging light sources including 365 nm UV, blue and red LED. UV light facilitated the visible PersL of Pr while the red light charged PersL was dominated by the NIR PersL of Tm. The UV-charged visible PersL of Pr and visible-light-charged NIR PersL of Tm might follow different mechanisms. UV light leads to cross band excitation and seems more efficient for Pr emission because its $^3P_0$ levels are close to the bottom of the conduction band. The visible light charging of Tm PersL at 800 nm seems more like a localized energy transfer process from Tm^{3+} to Ti^{3+} and oxygen vacancies with no cross band procedure, as shown in Figure S4. The charging process was further verified by using TSL (Figure 6B). Long excitation time is useful to increase the charged energy. The red-light-charging process reached a satu-

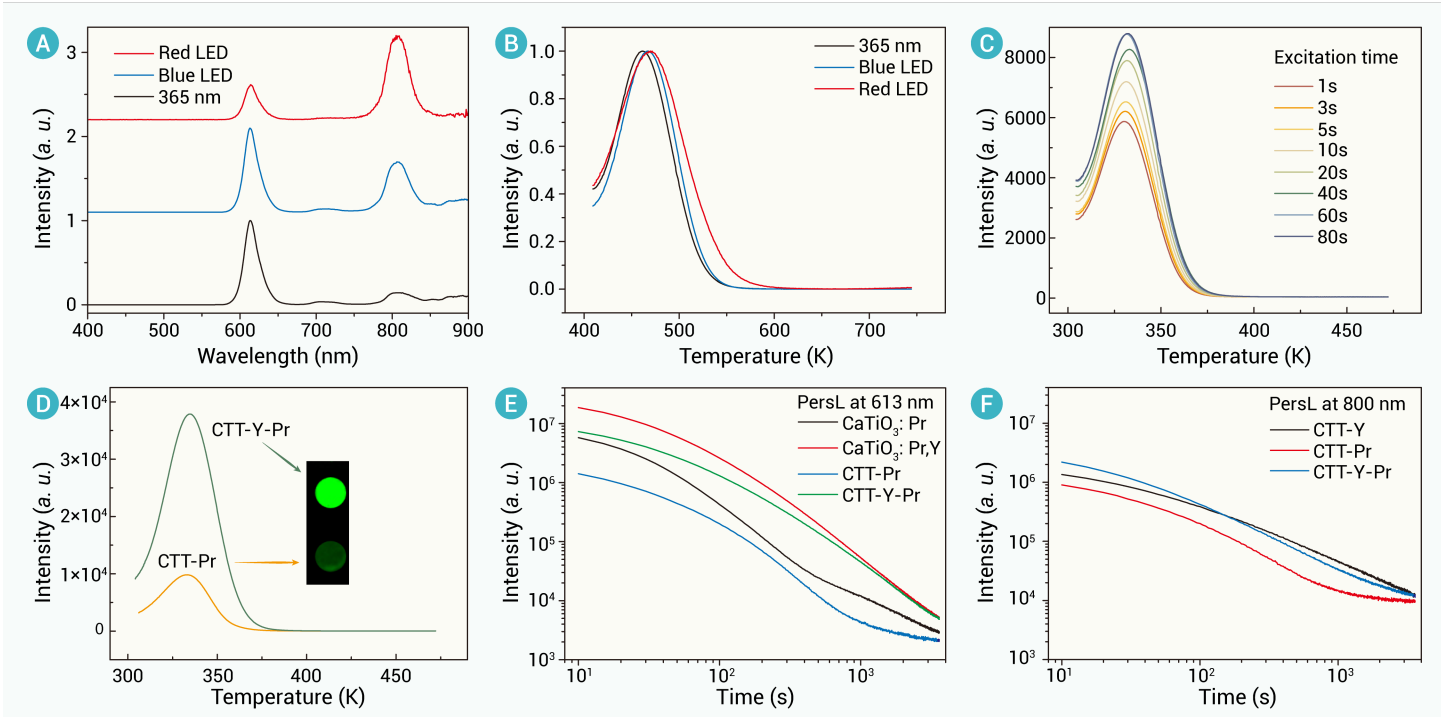

Figure 6. Visible-NIR double band PersL of CTT-Y-Pr (A) PersL spectra charged by using diverse light sources; (B) TSL after being charged by diverse light sources; (C) excitation time-dependence of red-light charged TSL intensity (delay, 20 s); (D) a comparison of the red-light charged TSL intensity of CTT-Y-Pr with CTT-Pr showing the influence of Y (delay, 2 s); (E) visible (613 nm) and (F) NIR (800 nm) PersL decay curves comparing with other related doped $CaTiO_3$ phosphors.

rated PersL intensity at ~ 60 s. Further increasing the charging time didn't increase the PersL intensity any more (Figure 6C). CTT-Y-Pr was compared with CTT-Pr by conduct a PersL imaging and testing the TSL. The results clearly showed its superior PersL property and thus verified the unique role of Y (Figure 6D). Regarding to the PersL of Pr at 613 nm, a significant enhancement was observed when comparing $CaTiO_3$:Pr,Y with $CaTiO_3$:Pr (Figure 6E). Although the PersL of CTT-Y-Pr at 613 nm was also weaker than $CaTiO_3$:Pr,Y, it is still more intense than that of $CaTiO_3$:Pr and much more intense than that of CTT-Pr (~ 5 times). The excitation spectra of Pr indicate a slight red-shift, which will facilitate its excitation by UV or even violet-blue light (Figure S5). Moreover, CTT-Y-Pr exhibited the most intense initial NIR PersL which is about ~ 2 times of CTT-Pr (Figure 6F). Although, CTT-Y-Pr decays a little faster than CTT-Y, the initial PersL intensity is more important when considering its rechargeable PersL by biocompatible red light. As rare earth-activated NIR PersL phosphors are still rare to date, a simple strategy to improve existing ones is significant to promote its diverse applications. CTT-Y-Pr has unusual visible-light rechargeable NIR PersL properties when comparing with existing NIR PersL materials that need X-ray excitation.[36-38] Thus, CTT-Y-Pr will find promising applications in lots of research fields such as bioimaging, luminescent analysis, information storage, encryption, and anti-counterfeiting.[39-43]

Multi-level optical anti-counterfeiting of CTT-Y, $CaTiO_3$:Pr, and CTT-Y-Pr

A 3-D printed dented pattern was prepared by filling the refined powder of CTT-Y and CTT-Y-Pr into its different parts to form a luminescent anti-counterfeiting logo (Figure 7A). Under 365 nm UV light, red fluorescence from Pr^{3+} was observed from CTT-Y-Pr. After turning off the UV, the red PersL pattern could be observed by naked eyes (Figures 7B-C). Notably, neither the NIR fluorescence nor the PersL of CTT-Y was observable to naked eyes, thus the pattern formed by CTT-Y was invisible. To acquire a whole luminescent pattern, a CCD camera had to be applied, as shown in Figure 7D. In addition, the NIR fluorescence could be excited by red LED, thus a NIR fluorescence image of the whole pattern could also be captured in a NIR fluorescence mode by using a 780 nm long pass filter (Figure 7E). In addition, the NIR or the visible PersL could be also charged efficiently by sun light, special charging light sources are not necessary to activate its NIR PersL (Figures 7F-G). Or, its NIR PersL at 800 nm is always being activated at common living environments with any lights. As a result, the as-prepared logo realized four level optical information by providing visible fluorescence, visible PersL, invisible NIR fluorescence, and invisible NIR PersL, which endows its potential application in anti-counterfeiting, optical information storage and encryption.

Potential application of CTT-Y-Pr for medical implant imaging

Tissue filler has important medical applications in plastic and reconstructive surgery. Its post-surgical imaging is required for regular safety evaluation. X-ray contrast reagents are currently added in tissue filler products for CT-imaging. As optical imaging is more bio-compatible, CTT-Y-Pr has potential to be used as a PersL imaging contrast reagent, so that the labeled tissue filler can be imaged via NIR PersL imaging by using red light illumination instead of X-ray. As a proof-of-concept, refined CTT-Y-Pr powder (prepared using a ball grinding mill with a diameter range of ~ 0.1-1 μm, Figure 8A) was added (1% by mass) into liquid medical silicone to endow it with visible fluorescence and NIR PersL properties (Figure 8B). The as-prepared CTT-Y-Pr particles were small enough to prepare an injectable tissue filler (Figure 8C). The silicone was then injected subcutaneously into a living mouse at 4 difference sites (No.1-4) with volumes of 100, 50, 25, 10 μL, respectively. As the ~800 nm fluorescence of Tm can be excited at 688 nm, a fluorescence image was captured by using a closing setup of 675/820 nm (Figure 8D). However, only injected sites of No. 1-3 with relatively big volumes could be identified easily. Notably, the PersL imaging realized a much higher signal to background (S/B) ratio of 123 comparing with that of the fluorescence imaging (S/B, 13). Thus, the missing No.4 injection with a 10 μL silicone volume was found only via PersL imaging in Figure 8E, indicating its advantage for *in vivo* imaging. Moreover, CTT-Y-Pr showed good biocompatibility to multiple cell lines including human liver cell, Hep G2, mouse fibroblast cell, L929, and mouse breast cell, 4T1, even at high concentrations up to 200 μg/L, while low toxicity was observed when culturing with human osteosarcoma cell, 143B, at concentrations higher than 50 μg/L (Figure S6). After 28 day implantation of the PersL tissue filler (100 μL), no significant

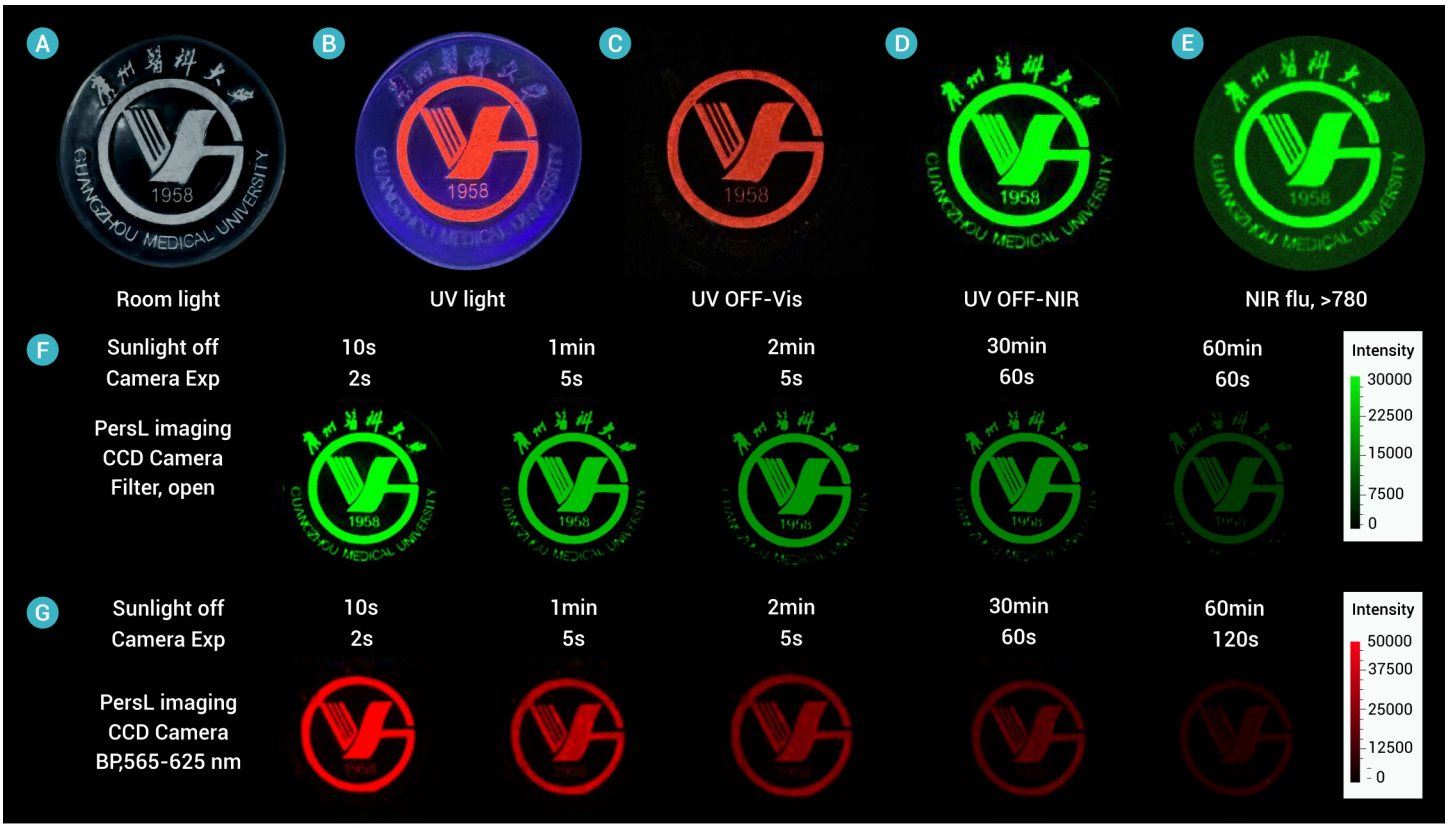

Figure 7. Multi-modal optical anti-counterfeiting based on CTT-Y and CTT-Y-Pr. Digital images taken by a cellphone camera (A) under room light, (B) under 365 nm UV light, (C) after turning off the UV light; NIR images taken by a CCD camera (D) PersL after turning off the UV light, (E) fluorescence under red light excitation, (F) PersL images with no filter or (G) a band pass filter (565-625 nm) captured by using a CCD camera after being illuminated by sun light for 10 s.

damage could be observed in the heart, liver, spleen, lung, kidney, and adjacent muscle of injected cite (Figure S7). Sometimes, the implanted tissue filler need to be taken out because of severe inflammation, deforming, and broken, etc. In this case, optical imaging is able to provide a real time guidance for tissue cleaning of tissue filler debris (Figure 8F). During tissue cleaning, the implanted silicone gel could be clearly seen by naked eyes and captured by using a common cell phone camera because of the intense red fluorescence of Pr at 613 nm (Figure 8G & Video S1). Interestingly, an unexpected tiny piece at site 5 was found via fluorescence, which was possibly caused by flowing of the injected silicone before its gelation. Guided by visible fluorescence, all the implanted silicone gel debris (No.1-4) and the unexpected tiny piece No.5 were successfully cleaned up from mouse body (Figures 8H-I). Notably, widely applied in clinical medicine, CT-imaging usually needs a long time to complete and has a limited sensitivity to targets smaller than 1 mm. The application of CTT-Y-Pr as a visible-NIR double band fluorescence and PersL imaging contrast will facilitate the post-surgical imaging evaluation of implanted tissue filler and the potential tissue cleaning. In addition to medical silicone, a lot of polymers are being used in clinical medicine, such as polyethylene in bone articulation, PMMA in bone cement, poly(tetrafluoroethylene) in artificial blood vessel and polyetheretherketone in bone screw. Instead of adding X-ray imaging contrasts, the reported PersL CTT-Y-Pr provides a new choice as an optical imaging contrast, as PersL imaging has no irradiation safety concern and can be applied more frequently, timely, and safely.

CONCLUSION

$CaTiO_3$:Tm,Y,Pr (CTT-Y-Pr) is developed with enhanced visible-NIR double band PersL property that is rechargeable by a wide spectrum from UV to red. Y-doping is a useful method to enhance the NIR PersL of Tm by 2 times and the visible PersL of Pr by 5 times in perovskite $CaTiO_3$ when comparing CTT-Y-Pr with CTT-Pr, which outstands other non-luminescent rare earth and boron group ions. Some basic laws are established in optimizing the NIR PersL of $CaTiO_3$:Tm (CTT) by choosing a proper co-dopant, which includes the doping at the A site of the ABO_3 structure, the rule of similar ionic radii, and the preference of a similar atomic number. The unique visible-NIR double band PersL attribute endows CTT-Y-Pr with potential applications not only in a four modal optical imaging for anti-counterfeiting but also a visible fluorescence-NIR PersL dual modal bio-imaging for tissue filler implantation and cleaning. As lanthanide ions have abundant spectra in the NIR, multi-band PersL will be possible to be extended to NIR-II in rare earth-doped $CaTiO_3$ and thus provide new choices to classic gallate-based NIR-I and II PersL materials.[44] This study provides a visible-NIR double band fluorescence-PersL material rechargeable by red light, develops some basic laws in designing latent NIR PersL materials with perovskite-like structures, and will be significant in exploring novel applications of PersL materials in optics and bio-optics.

REFERENCES

1. Jin L., Mo W., Wang Z., et al. (2025). Day-long organic persistent luminescence in flexible polymeric materials. *Angew. Chem. Int. Edit.* **64**:e202506261. DOI:10.1002/anie.202506261
2. Lin P., Shi J., Liu L., et al. (2025). Spatial confinement growth of high-performance persistent luminescence nanoparticles for image-guided sonodynamic therapy. *Acta Biomater.* **192**:279–289. DOI:10.1016/j.actbio.2024.12.011
3. Wang R., Shi J., Luo X., et al. (2025). Magnetic persistent luminescence nanoparticles repolarize tumor-associated macrophages for enhanced cancer immunotherapy. *ACS Materials Lett.* **7**:2094–2104. DOI:10.1021/acsmaterialslett.5c00170
4. Yao B., Xu F., Tian Z., et al. (2025). Strong persistent luminescence $NaYF_4$-based nanoparticles combined with manipulated hyperfractionated irradiation for X-ray-excited photodynamic therapy enhancement. *ACS Appl. Mater. Inter.* **17**:16561–16575. DOI:10.1021/acsami.4c20049
5. Zhou L., Chen R., Li X., et al. (2025). Multicolor persistent luminescence for high-sensitivity optical temperature sensing, human motion detection, and multimodal anticounterfeiting materials. *ACS Appl. Mater. Inter.* **17**:25451–25466. DOI:10.1021/acsami.5c01483
6. Abulipizi G., Yu Z., Lin S., et al. (2023). Trap engineering in $LiInSi_2O_6$:Cr,Pr by excess cristobalite silica for X-ray activated near-infrared persistent luminescence imaging

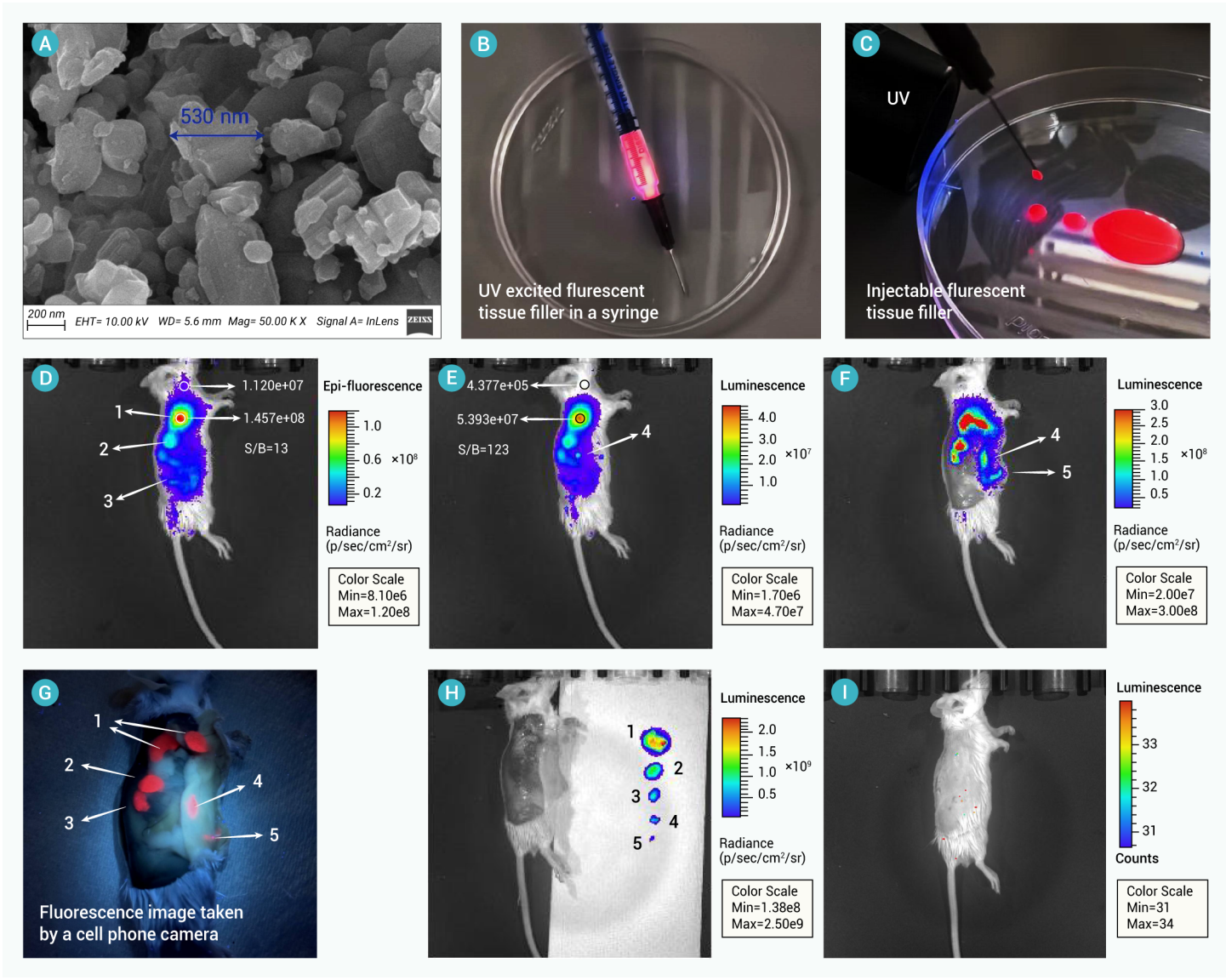

Figure 8. PersL imaging of CTT-Y-Pr labeled silicone tissue filler (A) Scanning electron microscopic image of CTT-Y-Pr; (B) CTT-Y-Pr/medical silicone tissue filler in a syringe under 365 nm excitation; (C) a fluorescent image showing injectable fluorescent tissue filler; (D) Fluorescence imaging (Ex/Em, 675/820 nm); (E) PersL imaging before surgical tissue cleaning; (F) PersL imaging of tissue filler debris during surgical tissue cleaning; (G) real time UV-excited visible fluorescence imaging during surgery; (H) imaging guided tissue cleaning of silicone debris; (I) post-operative PersL imaging evaluation of successful cleaning. The exposure times of (D-F), (H) and (I) were only 1 s.

in vivo. *Ceram. Int.* **49**:39664–39670. DOI:10.1016/j.ceramint.2023.09.321
7. Chen K., Xiong Y., Wang D., et al. (2024). A facile strategy for achieving polymeric afterglow materials with wide color-tunability and persistent near-infrared luminescence. *Adv. Funct. Mater.* **34**:202312883. DOI:10.1002/adfm.202312883
8. Feng Y., Yang X., Rao Q., et al. (2024). Persistent luminescence lifetime-based near-infrared nanoplatform via deep learning for high-fidelity biosensing of hypochlorite. *Anal. Chem.* **96**:7240–7247. DOI:10.1021/acs.analchem.4c00899
9. Luo X., Shi J., Wang R., et al. (2024). Near-infrared persistent luminescence nanoprobe for early detection of atherosclerotic plaque. *ACS Nano* **18**:6500–6512. DOI:10.1021/acsnano.3c12136
10. Wang Y., Zhang P., Tian X., et al. (2025). Persistent scintillators for X-ray repetitive imaging with stable energy traps. *J. Rare Earth.* **43**:1161–1168. DOI:10.1016/j.jre.2025.01.002
11. Yan L.-X., Yan Z.-Y., Zhao X., et al. (2024). Size-independent boosting of near-infrared persistent luminescence in nano-phosphors via a magnesium doping strategy. *J. Colloid. Interf. Sci.* **662**:11–18. DOI:10.1016/j.jcis.2024.02.008
12. Zhu Y., Wen Y., Xie Y., et al. (2025). Intelligent hierarchical targeting near-infrared persistent luminescence nanosystem for improved nuclear delivery and simultaneous visualization/therapy of EBV-associated cancer. *ACS Appl. Mater. Inter.* **17**:3072–3083. DOI:10.1021/acsami.4c20023
13. Zhu Q., Xiahou J., Guo Y., et al. (2019). $Zn_3Ga_2Ge_2O_{10}:Cr^{3+}$ uniform microspheres: Template-free synthesis, tunable bandgap/trap depth, and in vivo rechargeable near-infrared-persistent luminescence. *ACS App. Bio. Mater.* **2**:577–587. DOI:10.1021/acsabm.8b00734
14. Maldiney T., Bessiere A., Seguin J., et al. (2014). The *in vivo* activation of persistent nanophosphors for optical imaging of vascularization, tumours and grafted cells. *Nat. Mater.* **13**:418–426. DOI:10.1038/Nmat3908
15. Miao S. H., Lv X. L., Shan X. H., et al. (2024). Ultraviolet-B and near-infrared dual-band luminescence in Bi^{2+}/Bi^{3+} codoped persistent phosphor for optical storage application. *ACS Appl. Mater. Interfaces* **16**:23585–23595. DOI:10.1021/acsami.4c02522
16. Ding Y. C., So B., Cao J. K., et al. (2023). Light delivery, acoustic read-out, and optical thermometry using ultrasound-induced mechanoluminescence and the near-infrared persistent luminescence of CaZnOS:Nd. *Adv. Opt. Mater.* **11**:202300331. DOI:10.1002/adom.202300331
17. Su J. Y., Pang R., Tan T., et al. (2024). A novel near-infrared emitting $Sr_2LuSbO_6:Fe^{3+}$ phosphor with persistent luminescence performance. *Adv. Opt. Mater.* **12**:202303187. DOI:10.1002/adom.202303187
18. Zhou Z. H., He F. Q., Song E. H., et al. (2023). Broadband and multimode near-infrared emitter based on Cr^{3+}-activated stannate for multifunctional applications. *Adv. Opt. Mater.* **11**:202202466. DOI:10.1002/adom.202202466
19. Zhao Y. L., Wang X. D., Wang Q. H., et al. (2024). Abnormal spectral broadening of ordered-structure near-infrared phosphor $La_2CaHfO_6:Cr^{3+}$. *J. Mater. Chem. C* **12**:10532–10539. DOI:10.1039/d4tc01036a
20. Pan L., Delaey M., Wang Y., et al. (2024). Structural and optical properties of Cr ion-doped near-infrared long persistent luminescence silicogermanate phosphors with broad emission bands. *J. Alloy. Compd.* **983**:173853. DOI:10.1016/j.jallcom.2024.173853
21. Huang L., Lin L., Xie W., et al. (2020). Near-infrared persistent luminescence in a Cr^{3+}-

doped perovskite for low-irradiance imaging. *Chem. Mater.* **32**:5579–5588. DOI:10.1021/acs.chemmater.0c00807
22. Abulipizi G., Wang Y. X., Fang Y. L., et al. (2025). Persistent luminescent $NaYTi_2O_6$:Cr activated in the near-infrared bio-imaging window as a self-luminescent ceramic coating for visible Ti-implant *in vivo*. *Ceram. Int.* **51**:6959–6967. DOI:10.1016/j.ceramint.2024.12.130
23. Yu Z., Abulipizi G., Xu Y., et al. (2024). Stabilization of Ti^{3+} in $CaTiO_3$ by doping Y^{3+} to generate visible light-activated near-infrared persistent luminescence. *J. Alloy. Compd.* **983**:173879. DOI:10.1016/j.jallcom.2024.173879
24. Xu Y., Abulipizi G., Wang Y., et al. (2024). Near-infrared persistent luminescence of $CaTiO_3$:Cr,Y for imaging of bone implants using red-light illumination instead of X-ray. *ACS Appl. Mater. Interfaces* **16**:55823–55831. DOI:10.1021/acsami.4c13865
25. Abulipizi G., Zhou J., Qu C., et al. (2025). Unusual single band 803 nm persistent luminescence of Tm-doped calcium titanate charged in the near-infrared bio-imaging window. *ACS Appl. Mater. Interfaces* **17**:36912–36921. DOI:10.1021/acsami.5c07800
26. Kamioka H., Igarashi A., Watabe K., et al. (2025). Pr and Al doping effects on the red emission and long lasting afterglow in $CaTiO_3$ single crystals. *Opt. Mater.* **159**:116663. DOI:10.1016/j.optmat.2025.116663
27. Yin S., Chen D. and Tang W. (2007). Combustion synthesis and luminescent properties of $CaTiO_3$:Pr, Al persistent phosphors. *J. Alloy. Compd.* **441**:327–331. DOI:10.1016/j.jallcom.2006.09.120
28. Huang K., Li Z. J., Li Y., et al. (2021). Three-dimensional colloidal controlled growth of core-shell heterostructured persistent luminescence nanocrystals. *Nano Lett.* **21**:4903–4910. DOI:10.1021/acs.nanolett.0c04940
29. Qiao J. W., Zhang S., Zhou X. Q., et al. (2022). Near-infrared light-emitting diodes utilizing a Europium-activated calcium oxide phosphor with external quantum efficiency of up to 54.7%. *Adv. Mater.* **34**:202201887. DOI:10.1002/adma.202201887.
30. Liu L., Shi J. P., Wang J. Y., et al. (2024). Biodegradable persistent luminescence nanoparticles as pyroptosis inducer for high-efficiency tumor immunotherapy. *Adv. Sci.* **11**:202406340. DOI:10.1002/advs.202406340
31. Rakov N., Matias F. and Xiao M. F. (2024). An efficient red light-emissive process from Eu^{3+} doped amorphous-derived $CaAl_2Si_2O_8$ ceramic powders: Down-shifted luminescence with high thermal stability under 532 nm excitation. *Ceram. Int.* **50**:16064–16075. DOI:10.1016/j.ceramint.2024.02.086
32. V. Nikiforov I., V. Iliina E., Lazoryak B. I., et al. (2024). Photoluminescence, structural and antibacterial properties of co-doped β-$Ca_3(PO_4)_2$-type phosphates $Ca_8CuRE(PO_4)_7$ (RE = Eu-Er). *J. Rare. Earth.* **42**:1658–1668. DOI:10.1016/j.jre.2023.07.023
33. Van H. N., Cuong L. T., Nguyen D.-H., et al. (2025). Effect of Sr substituted on multifunction pure green emission of rare-earth-element doped HA/β-TCP nanocomposite for optical thermometer. *Ceram. Int.* **51**:16894–16903. DOI:10.1016/j.ceramint.2024.07.119
34. Piotrowski W. M., Ristic Z., Dramicanin M. D., et al. (2022). Modification of the thermometric performance of the lifetime-based luminescent thermometer exploiting Ti3+ emission in SrTiO3 and CaTiO3 by doping with lanthanide ions. *J. Alloy. Compd.* **906**:164398. DOI:10.1016/j.jallcom.2022.164398
35. Chen Y. F. and Pan Z. W. (2023). Red/NIR/SWIR multi-band persistent luminescent nanoparticles as ultrasensitive multi-channel tracers in water and crude oil/water emulsions. *Nano Res.* **16**:12706–12712. DOI:10.1007/s12274-023-6116-x
36. Yin X., Zhong H., Liu L., et al. (2024). X-ray-activated Bi^{3+}/Pr^{3+} co-doped $LiYGeO_4$ phosphor with UV and NIR dual-emissive persistent luminescence. *J. Rare Earth.* **42**:955–961. DOI:10.1016/j.jre.2023.03.008
37. Zhao T., Sun W., Wang S., et al. (2025). Low-dose X-ray induced long afterglow NIR luminescence from Cr^{3+} doped $Zn_{1-x}Cd_xGa_2O_4$ spinel solid solutions. *J. Rare Earth.* **43**:246–252. DOI:10.1016/j.jre.2023.12.006
38. Wang Y., Abulipizi G., Zhou J., et al. (2025). Persistent luminescence of Dy-doped strontium pyrophosphate with double traps for room temperature qualitative and heated quantitative X-ray dosimetry by naked eyes. *J. Alloy. Compd.* **1022**:179900. DOI:10.1016/j.jallcom.2025.179900
39. Gao L., Liu Y., Su J., et al. (2025). Modulation of near-infrared afterglow luminescence in inorganic nanomaterials for biological applications. *Adv. Mater.* **37**:202419349. DOI:10.1002/adma.202419349
40. Shang R., Yang F., Gao G., et al. (2024). Bioimaging and prospects of night pearls-based persistence phosphors in cancer diagnostics. *Exploration* **4**:20230124–20230124. DOI:10.1002/exp.20230124
41. Wei Y. and Wang J. (2024). X-ray/γ-ray/ultrasound-activated persistent luminescence phosphors for deep tissue bioimaging and therapy. *ACS Appl. Mater. Interfaces* **16**:56519–56544. DOI:10.1021/acsami.4c11585
42. Yang X., Waterhouse G. I. N., Lu S., et al. (2023). Recent advances in the design of afterglow materials: mechanisms, structural regulation strategies and applications. *Chem. Soc. Rev.* **52**:8005–8058. DOI:10.1039/d2cs00993e
43. Cai G. Y., Delgado T., Richard C., et al. (2023). ZGSO Spinel nanoparticles with dual emission of NIR persistent luminescence for anti-counterfeiting applications. *Materials* **16**:1132. DOI:10.3390/ma16031132
44. Cai G. Y., Naillon T., Seguin J., et al. (2024). ZGSO:Cr^{3+}, Ni^{2+} persistent phosphors with dual emission in NIR-I and SWIR ranges for bio-imaging applications. *Small* **20**:202406507. DOI:10.1002/smll.202406507

FUNDING AND ACKNOWLEDGMENTS

This research was supported by the National Natural Science Foundation of China (grant numbers 52172277). We thank the Scientific Research Center of the Guangzhou Medical University for the assistance on the animal imaging service. The funders had no role in study design, data collection and analysis, decision to publish, or preparation of the manuscript.

AUTHOR CONTRIBUTIONS

Conceptualization: Juanjuan Zhou, Leping Ding Methodology: Leping Ding. Data curation: Leping Ding, Gulizhabaier Abulipizi, Chaomin Qu, Ziang Zong, Yanlun Fang, Yawen Zheng, Xingyuan Shi. Formal analysis: Leping Ding. Funding acquisition: Zhanjun Li. Project administration: Zhanjun Li. Supervision: Zhanjun Li. Writing – original draft: Leping Ding, Juanjuan Zhou. Writing – review & editing: Zhanjun Li. All authors contributed to the manuscript and approved the final version.

DECLARATION OF INTERESTS

The authors declare no competing interests.

ETHICAL STATEMENT AND PATIENT CONSENT

All animal procedures were applied per a protocol approved by the Institutional Animal Care and Use Committee of Guangzhou Medical University (GY2024-633).

DATA AND CODE AVAILABILITY

Data are available from the corresponding author upon reasonable request.

SUPPLEMENTAL INFORMATION

It can be found online at https://doi.org/10.59717/j.xinn-mater.2026.100200.